



This discussion paper is/has been under review for the journal Atmospheric Chemistry and Physics (ACP). Please refer to the corresponding final paper in ACP if available.

Estimating sources of elemental and organic carbon and their temporal emission patterns using a Least Squares Inverse model and hourly measurements from the St. Louis-Midwest Supersite

B. de Foy¹, Y. Y. Cui^{1,2}, J. J. Schauer³, M. Janssen⁴, J. R. Turner⁵, and C. Wiedinmyer⁶

¹Department of Earth and Atmospheric Sciences, Saint Louis University, MO, USA

²Chemical Sciences Division, Earth System Research Laboratory, National Oceanic and Atmospheric Administration (NOAA), Boulder, CO, USA

³Civil and Environmental Engineering, University of Wisconsin – Madison, WI, USA

⁴Lake Michigan Air Directors Consortium (LADCO), Rosemont, IL, USA

⁵Energy, Environmental and Chemical Engineering Department, Washington University in St. Louis, MO, USA

⁶National Center of Atmospheric Research, Boulder, CO, USA

Title Page

Abstract

Introduction

Conclusions

References

Tables

Figures

◀

▶

◀

▶

Back

Close

Full Screen / Esc

Printer-friendly Version

Interactive Discussion



Received: 26 March 2014 – Accepted: 29 April 2014 – Published: 13 May 2014

Correspondence to: B. de Foy (bdefoy@slu.edu)

Published by Copernicus Publications on behalf of the European Geosciences Union.

ACPD

14, 12019–12070, 2014

EC and OC inverse modeling

B. de Foy et al.

Title Page

Abstract

Introduction

Conclusions

References

Tables

Figures

◀

▶

◀

▶

Back

Close

Full Screen / Esc

Printer-friendly Version

Interactive Discussion



Abstract

An inverse model was used to evaluate emission inventories of Elemental Carbon (EC) and Organic Carbon (OC) based on year-long hourly time series from the St. Louis-Midwest Supersite. The input to the model consisted of continuous measurements of EC and OC obtained for 2002 using two semicontinuous analyzers. High resolution meteorological simulations were performed for the entire time period using the Weather Research and Forecasting model (WRF). These were used to simulate hourly back-trajectories at the measurement site using a Lagrangian model (FLEXPART-WRF). In combination, an Eulerian model (CAMx) was used to simulate the impacts at the measurement site using known emissions inventories for point and area sources as well as for open burning. By considering only passive transport of pollutants, and by using diagonal error covariance matrices, the Bayesian inversion simplifies to a single least squares inversion. The inverse model combines forward Eulerian simulations with backward Lagrangian simulations to yield estimates of emissions from sources in current inventories as well as from area emissions that might be missing in the inventories. The CAMx impacts were disaggregated into separate time chunks in order to determine improved diurnal, weekday and monthly temporal patterns of emissions. Because EC is a primary species, the inverse model estimates can be interpreted directly as emissions. In contrast, OC is both a primary and a secondary species. As the inverse model does not differentiate between direct emissions and formation in the plume of those direct emissions, the estimates need to be interpreted as contributions to measured concentrations. Emissions in the St. Louis region from On-Road, Non-Road, Marine/Aircraft/Railroad (MAR), "Other" and Point Sources were revised slightly downwards on average. In particular, both MAR and Point Sources had a more pronounced diurnal variation than in the inventory. The winter peak in Other emissions was not corroborated by the inverse model. On-Road emissions have a larger difference between weekday and weekends in the inverse estimates than in the inventory, and appear to be poorly simulated or characterized in the winter months. The model

EC and OC inverse modeling

B. de Foy et al.

Title Page

Abstract

Introduction

Conclusions

References

Tables

Figures

◀

▶

◀

▶

Back

Close

Full Screen / Esc

Printer-friendly Version

Interactive Discussion



EC and OC inverse modeling

B. de Foy et al.

Title Page

Abstract

Introduction

Conclusions

References

Tables

Figures

◀

▶

◀

▶

Back

Close

Full Screen / Esc

Printer-friendly Version

Interactive Discussion



misattributing impacts from distinct sources due to compensating errors in models, as also described in Napelenok et al. (2014). In Milwaukee, de Foy et al. (2012a) found that EC levels were predominantly due to mobile sources, although simulations suggested that 10 % could be due to shipping emissions from the Port of Milwaukee. While EC levels are clearly associated with mobile sources, the ratios of EC to other pollutants can vary between cities and there is therefore a clear need to improve monitoring of EC and OC in order to improve emissions inventories (Reche et al., 2011). This is illustrated by Gentner et al. (2012) who evaluate the different contributions of gasoline and diesel vehicles to secondary organic aerosol concentrations.

The present study is based on continuous, hourly measurements of EC and OC made during 2002 at the St. Louis-Midwest Supersite (Bae et al., 2004b). Bae et al. (2004a) analyzed the temporal profiles of EC, OC and the EC to OC ratio. Both EC and OC have minimum concentrations from February to May. OC has maximum concentrations during the summer whereas EC has maximum concentrations during the fall. EC was found to vary by day of week with a mid-week maximum and a minimum on Sundays. Furthermore, EC had peak concentrations in the morning and early evening. In contrast, OC does not vary by day of week and has a different diurnal pattern than EC, with lower concentrations during the early afternoon. Analysis of the EC to OC ratio suggest that the morning peak in EC is related to traffic emissions, but that the evening peak may be due to meteorological factors. Measurements of water-soluble OC (Sullivan et al., 2004) suggested that a significant fraction of the OC is from secondary organic aerosol formation, in agreement with the different temporal profiles of OC and EC at the measurement site. Sheesley et al. (2007) further analyzed the EC and OC data along with organic tracers. In addition to detecting impacts from point sources, they found differences in the temporal profiles in St. Louis with those of southern California. Bae et al. (2006) used 24 h averaged data for source attribution of OC. This identified a significant component of OC due to wood smoke and to smoking vehicles. Jaeckels et al. (2007) used Positive Matrix Factorization to identify contributions to OC concentrations. They likewise found a strong component of wood combustion

and secondary organic aerosol. In addition, they identified a mobile factor which has a strong monthly variation.

Cluster analysis of PM_{2.5} composition has shown that St. Louis has similar aerosol composition as other industrial midwest cities such as Chicago, Detroit and Cleveland (Austin et al., 2013). The St. Louis-Midwest Supersite is impacted by metal processing point sources to the southwest, as shown using wind roses and conditional probability functions by Amato and Hopke (2012); Wang et al. (2011); Lee et al. (2006); Lee and Hopke (2006). These studies also confirmed the regional nature of OC, with source regions broadly from the southeast and southwest quadrant. EC has a similar signature although it is less homogeneous and points to more source directions. Potential source contribution function used back-trajectories to show that sulfate levels at the site were impacted by the Ohio River Valley, while nitrate levels were associated with transport from the west and northwest.

In this paper we use an inverse model to identify sources using a year-long hourly time series of EC and OC measured in East St. Louis. The model estimates the diurnal and monthly emission profiles of five different source categories as well as the emissions from open burning. In addition, the inverse model uses gridded back-trajectories to identify regions that may be missing sources in the inventory. As discussed above, EC is transported in the atmosphere, but OC is both emitted and created. Our model is focused on transport and consequently the results for EC can be straightforwardly compared to emission inventories. For OC however, the model does not distinguish between primary OC that is emitted by a source and secondary OC that is created in the plume of that same source. The results are therefore best interpreted in terms of impacts at the measurement site rather than emissions at the source location.

EC and OC inverse modeling

B. de Foy et al.

Title Page

Abstract

Introduction

Conclusions

References

Tables

Figures

◀

▶

◀

▶

Back

Close

Full Screen / Esc

Printer-friendly Version

Interactive Discussion



EC and OC inverse modeling

B. de Foy et al.

Title Page

Abstract

Introduction

Conclusions

References

Tables

Figures

◀

▶

◀

▶

Back

Close

Full Screen / Esc

Printer-friendly Version

Interactive Discussion



updated temporal profiles. Mobile emissions were estimated using the MOVES2010a model (EPA, 2012). Non-Road emissions were updated to reflect higher agricultural equipment emissions during the spring and fall season rather than the default of a single summer maximum. For EC and OC, Other sources consist mainly of residential wood and waste combustion with smaller contributions from unpaved roads, food preparation and construction.

Figure 2 shows the emissions for EC in metric tonnes per year (tpy). OC emissions have similar patterns with the following average OC to EC ratios: 0.62 for On-Road, 0.64 for Non-Road, 0.49 for MAR, 6.7 for Other and 2.5 for Point Sources. Table 2 presents the emission totals for the Regional domain shown in Fig. 1.

Biogenic emissions in LADCO (2011) were calculated using the Model of Emissions of Gases and Aerosols from Nature (MEGAN) version 2.03a (Guenther et al., 2006). As an example, Fig. 2 shows the spatial map of the biogenic emissions of condensable gases, category “CG5” in non-dimensional units. These will be used as a tracer of biogenic emissions in the Eulerian simulations, and the concentrations will be normalized before being included in the inversion algorithm. As will be discussed in Sect. 3.2, the inverse results therefore do not represent an estimate of actual biogenic emissions, but rather an estimate of the fraction of OC that could be ascribed to aerosol formation due to these emissions.

The 2008 National Emissions Inventory (NEI) version 3 was obtained from the US Environmental Protection Agency. EC and OC emissions were available in specialized files for $PM_{2.5}$. The On-Road emissions in the NEI were calculated using the MOVES2010b model (EPA, 2012). The data was provided as annual totals by Federal Information Processing Standards (FIPS) codes. These were mapped to the Regional model grid in order to compare NEI emissions with the emissions in the LADCO prior and with the inverse model posterior. Although emission inventories existed for 2002, it was felt that the considerable improvements and developments that went into the LADCO 2007 inventory meant that this would be a better choice for the prior, and that consequently the 2008 NEI was the most appropriate comparison point to the prior.

EC and OC inverse modeling

B. de Foy et al.

[Title Page](#)[Abstract](#)[Introduction](#)[Conclusions](#)[References](#)[Tables](#)[Figures](#)[◀](#)[▶](#)[◀](#)[▶](#)[Back](#)[Close](#)[Full Screen / Esc](#)[Printer-friendly Version](#)[Interactive Discussion](#)

EC and OC emissions from open burning were calculated using the Fire Inventory from NCAR (FINN) version 1 (Wiedinmyer et al., 2011). FINN calculates daily emissions from fires identified by fire counts from the Terra Moderate Resolution Imaging Spectroradiometer (MODIS) fire and thermal anomalies data provided from the official NASA MCD14ML product, Collection 5, version 1 (Giglio et al., 2003). Land cover and vegetation density needed to calculate the emissions were determined with the MODIS Land Cover Type product (Friedl et al., 2010) and the MODIS Vegetation Continuous Fields product (Collection 3 for 2001) (Hansen et al., 2003, 2005; Carroll et al., 2011), and fuel loadings from Hoelzemann et al. (2004) and Akagi et al. (2011). Ecosystem-specific emission factors for EC and OC emissions were compiled from existing literature (Table 1, Wiedinmyer et al., 2011). Ratios of OC to EC emission factors range from 4.8 for fires in croplands, to 39 for fires in boreal forests. Daily emission totals were distributed evenly throughout the day as input to CAMx simulations.

In FINN, open burning includes the fires which are detected by Terra MODIS. These are a combination of forest fires, prescribed burns and larger agricultural fires, with a minimum burn area of 1 km². Hawbaker et al. (2008) analyzed the detection rate of MODIS compared to a set of reference fires. The rates were high when both Terra and Aqua were used, but dropped to 60 % in the Great Plains and 39 % in the eastern US when only Terra was used. Because we only have Terra data for 2002, this is an added source of uncertainty in the emission estimates.

Figure 3 shows the total gridded open burning emissions for 2002 on the Large model domain, and Table 3 shows the total emissions by sector. The inverse model calculated posterior emissions independently for the following 6 geographical sectors: local emissions within 100 km of the measurement site followed by the northeast, southeast, southwest, west and northwest as shown in Fig. 3. The largest emissions are in the southeast and southwest sector.

2.3 Numerical simulations

The meteorological simulations were performed with the Weather Research and Forecasting (WRF) model version 3.5.1 (Skamarock et al., 2005). The North American Regional Reanalysis (NARR) (Mesinger et al., 2006) was used for the initial and boundary conditions. The simulations used 3 domains with 27, 9 and 3 km horizontal resolution and 40 vertical levels. Figure 1 shows a map of the 3 domains, which will be referred to as the Large, the Regional and the Local domains.

The model was run with two-way nesting, with the Yonsei University (YSU) boundary layer scheme, the Kain–Fritsch convective parameterization, the NOAA land surface scheme, the WSM 3-class simple ice microphysics scheme, the Dudhia shortwave scheme and the Rapid Radiation Transfer Model longwave scheme. Individual simulations were performed lasting 162 h, of which the first 42 h were considered spin-up time and the remaining 5 days were used for analysis. The simulations are similar to those described in de Foy et al. (2014), where it was shown that the model accurately represents the statistical distribution of temperature, humidity, wind speed and wind direction at the surface (see Fig. 3 in de Foy et al., 2014).

Particle back-trajectories were calculated from the supersite with FLEXPART (Stohl et al., 2005), using FLEXPART-WRF (Brioude et al., 2013b) for a duration of 4 days starting every hour of the year using the WRF simulated wind fields. 1000 particles were released per hour between 0 and 100 m above the ground and were allowed to disperse in three dimensions using the WRF mixing heights and surface friction velocity. Sensitivity tests presented in de Foy et al. (2012b) found that 1000 particles were sufficient to ensure that the results did not depend on the number of particles for inversions on a regional scale. The particle positions were converted to polar grids to provide a Residence Time Analysis (RTA, Ashbaugh et al., 1985). This represents the amount of time that an air mass has spent in different grid cells before arriving at the measurement location and can be rescaled to yield the impact that a source in each grid cell would have at the receptor site (Seibert and Frank, 2004; Lin et al., 2003).

Title Page

Abstract

Introduction

Conclusions

References

Tables

Figures

◀

▶

◀

▶

Back

Close

Full Screen / Esc

Printer-friendly Version

Interactive Discussion



EC and OC inverse modeling

B. de Foy et al.

Title Page

Abstract

Introduction

Conclusions

References

Tables

Figures

◀

▶

◀

▶

Back

Close

Full Screen / Esc

Printer-friendly Version

Interactive Discussion



Concentration Field Analysis (CFA, Seibert et al., 1994; de Foy et al., 2009, 2007) was used as a preliminary method to evaluate possible source regions suggested by the Residence Time Analysis and the hourly concentrations. As described in Sect. 3.1 below, standard CFA is sensitive to peak concentrations, and so we apply the method to an estimate of the column amount of pollutant. This “Column CFA” is shown below to give a more reliable estimate of potential source regions than using CFA based on surface concentrations alone.

The Comprehensive Air-quality Model with eXtensions (CAMx v6.00, ENVIRON, 2013), an Eulerian 3-D grid model, was used to obtain hourly concentrations of EC and OC at the measurement site based on the prior emissions inventory. This study is focused on estimating source contributions from specific source groups based on atmospheric transport and therefore does not use the aerosol module in CAMx. For the LADCO inventory, CAMx was run with 2 nested domains: the Regional and the Local domains from the WRF simulations (shown in Fig. 1), whereas for open burning, CAMx was run with the Large and the Regional domains.

2.4 Least Squares Inverse model

The Least Squares Inverse model used in the present study was developed in de Foy et al. (2012b) and de Foy et al. (2014), where it was used to evaluate emissions inventories of elemental and reactive mercury. The inverse model estimates emissions that contribute to measured concentrations at a receptor site. This is done by using both the passive transport from prior sources and the contribution of unknown sources using gridded back-trajectories.

Inverse models based on back-trajectories alone include Stohl et al. (2009); Brioude et al. (2011, 2013a). This work combines back-trajectories with Eulerian simulations, and in this respect is similar to the two-step method (Rigby et al., 2011; Roedenbeck et al., 2009).

We simulate concentrations at the receptor sites using forward simulations from prior sources for different time periods. This study focuses on the temporal profile of different

EC and OC inverse modeling

B. de Foy et al.

Title Page

Abstract

Introduction

Conclusions

References

Tables

Figures

◀

▶

◀

▶

Back

Close

Full Screen / Esc

Printer-friendly Version

Interactive Discussion



types of source emissions: On-Road, Non-Road, MAR, Other and Point Sources. For each category, we perform simulations for weekdays and for Saturdays, Sundays and Holidays. These are further subdivided into runs for 5 different time slots during the day: 11:00 p.m. to 05:00 a.m., 05:00 a.m. to 08:00 a.m., 08:00 a.m. to 02:00 p.m., 02:00 p.m. to 06:00 p.m., and 06:00 p.m. to 11:00 p.m. These were selected based on the diurnal profile used in the emissions inventory. We therefore have 10 simulations for each of 5 source categories, and we divide the resulting concentration time series into 12 months for a total of 600 input time series into the inverse model. With this method of resolving temporal profiles, individual time series are used for each temporal interval of interest. This is in contrast with Brunner et al. (2012) who use a Kalman filter to identify seasonal changes in emissions.

The open burning emissions are included in the inversion as 6 time series covering the entire year for the 6 geographic sectors shown in Fig. 3. We also include a time series representing impacts from biogenic emissions, as discussed in Sect. 3.2.

In addition to the forward Eulerian simulations, we perform backward Lagrangian simulations of particle back-trajectories for each hour of the measurement campaign. These are mapped onto a polar grid surrounding the measurement site. The time series from each grid cell gives an estimate of the concentration at the measurement site that would be caused by a constant area emission in that cell. We divided these gridded time series into impacts due to weekdays and weekends, and also into 4 time slots during the day: 03:00 a.m. to 09:00 a.m., 09:00 a.m. to 03:00 p.m., 03:00 p.m. to 09:00 p.m., and 09:00 p.m. to 03:00 a.m. These were selected to capture the morning and afternoon rush hours in the middle of 2 of the slots, and to differentiate the daytime and nighttime emissions between those. The polar grid was chosen to have eighteen 20° segments, in 20 radial bands extending to 1000 km from the measurement site. There were therefore 360 time series from 8 time slots, for a total of 2880 time series to be used as input into the inverse model.

The Least Squares Inverse model derives a posterior estimate of emissions based on the emissions inventory used as a prior. It also derives an estimate of area sources

on the polar grids impacting the measurement site. A field of zero prior emissions is used for these as they are additional to the known sources in the emissions inventory.

By limiting the input of the model to passive tracers and individual time series, we can use a least squares simplification developed in de Foy et al. (2012b) to the Bayesian formulation used in Stohl et al. (2009). This hybrid least squares method derives an estimate of the emissions vector \mathbf{x} that minimizes the cost function J given by the sum of the observation cost function and the emissions cost function:

$$J = \|(\mathbf{H}\mathbf{x}' - \mathbf{y}')\|_2 + \alpha^2 \|\mathbf{x}'\|_2 \quad (1)$$

Where $\mathbf{x}' = \mathbf{x} - \mathbf{x}_o$ is the vector of adjustment factors given prior emissions estimates \mathbf{x}_o . \mathbf{H} is the sensitivity matrix that converts emissions parameters \mathbf{x} into simulated concentrations. Vector $\mathbf{y}' = \mathbf{y} - \mathbf{H}\mathbf{x}_o$ is the residual between the vector of concentration measurements \mathbf{y} and the time series produced by the prior emissions estimates $\mathbf{H}\mathbf{x}_o$. α is the regularization parameter that balances the two parts of the cost function. This method was shown to be equivalent to a Bayesian derivation when diagonal error covariance matrices are used (de Foy et al., 2012b; Wunsch, 2006; Aster et al., 2012). In these cases, the regularization parameter is equal to the ratio of the uncertainty of the measurements to the uncertainty of the emissions parameter, as described in de Foy et al. (2012b).

The columns of \mathbf{H} contain the 606 input time series from the forward Eulerian simulations (in the same units as the measurements) as well as the 2880 time series from the back-trajectory grids (in units relating area emissions to measurement concentrations, see de Foy et al., 2012b). The rows of \mathbf{H} correspond to the impact of the different sources for each of the 7091 h with valid data, which are contained in vector \mathbf{y} . The vector \mathbf{x} contains (606 + 2880) entries which yield the posterior emissions estimate for the source groups and for the gridded area sources represented by the back-trajectories. The entries in \mathbf{x} are scaling factors which yield posterior emissions estimates when they are multiplied by the prior emissions.

EC and OC inverse modeling

B. de Foy et al.

Title Page

Abstract Introduction

Conclusions References

Tables Figures

◀ ▶

◀ ▶

Back Close

Full Screen / Esc

Printer-friendly Version

Interactive Discussion



EC and OC inverse modeling

B. de Foy et al.

Title Page

Abstract

Introduction

Conclusions

References

Tables

Figures

◀

▶

◀

▶

Back

Close

Full Screen / Esc

Printer-friendly Version

Interactive Discussion



The system of equations can be solved with a single step of least squares using:

$$J = \|\mathbf{s} \cdot (\mathbf{H}'' \mathbf{x}' - \mathbf{y}'')\|_2 \quad (2)$$

Where $\mathbf{H}'' = (\mathbf{H}, \mathbf{I})$ and $\mathbf{y}'' = (\mathbf{y}', \mathbf{x}_{\text{zero}})^T$ are the augmented versions of \mathbf{H} and \mathbf{y}' . \mathbf{I} is the identity matrix the size of \mathbf{x} , and \mathbf{x}_{zero} is a vector of zero values. Hence, the first part of \mathbf{H}'' and of \mathbf{y}'' correspond to the observation cost function and the second part to the emissions vector cost function. The vector \mathbf{s} contains scaling factors on the parts of the cost function: these are taken to be unit values for the observation cost function and contain the regularization parameter α for the emissions cost function.

A strength of the method is that boundaries can be straightforwardly applied to the vector \mathbf{x}' during the least squares solution to prevent nonphysical negative emissions. An Iteratively Reweighted Least Squares (IRLS) scheme is used to reduce the sensitivity of the method to outliers in the data: after solving for \mathbf{x} , observation times that have a residual larger than 3 times the standard deviation of the residual values are removed from the analysis. This is performed iteratively to converge on a stable set of times to include in the inversion. EC and OC simulations were evaluated separately using the Least Squares Inverse model.

In a Bayesian framework, uncertainty estimates are required to obtain the error covariance matrices on the two parts of the cost function. In the absence of detailed prior information, Efron (2013) recommends using empirical Bayes methods where the prior information is obtained from the dataset itself. If this is insufficient, then using frequentist methods is recommended as a check on the Bayesian simulations. In this context, the current method can be understood as a frequentist method where the inversion is performed multiple times using bootstrapping, and where the regularization parameter is obtained from the data itself.

The Least Squares Inverse model therefore does not need prior error estimates, but rather relies on an optimization routine to determine the values of the regularization parameters in the vector \mathbf{s} that minimize the total error following Henze et al. (2009). These are determined separately for the emissions inventory sources, for the open

EC and OC inverse modeling

B. de Foy et al.

Title Page

Abstract

Introduction

Conclusions

References

Tables

Figures

◀

▶

◀

▶

Back

Close

Full Screen / Esc

Printer-friendly Version

Interactive Discussion



burning sources and for the emissions based on back-trajectories. The regularization parameter for the gridded emissions is scaled by the cell area to account for the increase in uncertainty with increasing distance from the measurement site. This yields values for the EC inversion of: 0.025 for gridded emissions, 1 for emissions inventory sources and 0.03 for open burning. The corresponding parameters for OC are: 0.015, 1, 0.25 and an additional parameter of 0.5 for the biogenic contribution. Taking the uncertainty of the measurements to be $1 \mu\text{g m}^{-3}$, this corresponds to an uncertainty of 100% for the emissions inventory sources, and to an uncertainty factor for open burning of 33 for EC and 4 for OC.

Miller et al. (2014) review different methods to enforce positive emissions in the inversion, and show that some of these may bias the results. In the Least Squares Inverse model, the inversion is performed by the function lsqin in Matlab. This uses a trust-region reflective Newton method to solve the least squares problem and enforce positive constraints on the results. This does not prevent the model from estimating uncertainties, as we derive a regularization parameter from the data and obtain the uncertainty estimates using bootstrapping.

The probability density distributions of the WRF parameters shown in Fig. 3 in de Foy et al. (2014) suggest that there are no systematic errors in the model. The autocorrelation of simulation errors has a time scale of less than 12 h. The uncertainty due to transport errors and the sensitivity to individual episodes can therefore be evaluated by using the blocked-bootstrap technique with a block length of 24 h. We perform 100 inversions with random selection with replacement of the days included in the analysis. In this way, the bootstrapping yields an estimate of the combined uncertainty due to measurement errors and due to transport modeling errors.

EC and OC inverse modeling

B. de Foy et al.

Title Page

Abstract

Introduction

Conclusions

References

Tables

Figures

◀

▶

◀

▶

Back

Close

Full Screen / Esc

Printer-friendly Version

Interactive Discussion



calm winds, and the remaining having winds predominantly from the southeast. Snyder et al. (2009) found an episode where high levels of Cadmium, Antimony, Barium and Selenium were associated with a very clear southeast signature. This could be due to a power station 53 km away in that direction, although simulations with CAMx did not support such high impacts from this source. Further analysis found that peak EC concentrations are associated with these hours with very stable vertical mixing conditions which themselves are associated with weak southeasterly transport. They appear to be linked to occurrences of the Low Level Jet. This suggests that micrometeorology needs to be taken into account when analyzing high pollution events in St. Louis.

Wind rose analysis and CFA are sensitive to peak concentrations occurring during situations with very shallow boundary layers and so we need to expand the methods to be more sensitive to the amount of pollutant rather than to the peak concentration. This can be done by calculating a “Column CFA”: CFA is carried out with an estimate of the total column of EC rather than with the surface concentration of EC. To do this, we assume that EC and OC are mainly in the planetary boundary layer and that concentrations are well mixed throughout. The column amount is obtained by multiplying the surface concentration by the height of the boundary layer. Since we do not have measurements of the mixing height, we use simulated values from the WRF model. The two graphs on the right in Fig. 6 show the results of the Column CFA for EC and OC. For EC, we can now see a clear signature from the St. Louis metropolitan area as well as a smaller signature from the Illinois side of the urban zone. For OC, the St. Louis metropolitan area shows up but there is a stronger signal of general impacts from both the southeast and the southwest, which is consistent with regional atmospheric formation of OC compared with local transport of EC.

3.2 Inverse model results: time series and impacts

Figure 4 shows the EC and OC time series of the measurements and of the inverse model results. The time series from the inverse model are much improved compared with those simulated using the emissions prior, as shown by the statistical measures

EC and OC inverse modeling

B. de Foy et al.

Title Page

Abstract

Introduction

Conclusions

References

Tables

Figures

◀

▶

◀

▶

Back

Close

Full Screen / Esc

Printer-friendly Version

Interactive Discussion



egory with 68 % of impacts, followed by Point Sources with 12 %, On-Road with 9 %, Non-Road with 6 %, and MAR and open burning with 3 % each. The posterior accounts for 88 % of the average OC levels, mainly by reducing the impacts of the source groups and using the RTA grids to represent 46 % of the impacts. Impacts from open burning are increased in the posterior so that they make up 5 % of the total OC.

Normalized time series of biogenic precursor concentrations were included in the analysis. Because the units are non-dimensional, the results from the inverse model give an indication of the fraction of EC or OC that correlates with these emissions, without giving an estimate of the emissions themselves. As expected, none of the biogenic precursors contributed to the EC time series in the inversion, and these were therefore left out of the EC inversions. For OC, condensable gases category 5 “CG5” yielded the most consistent estimate of impacts in the inversion. The model was therefore run just with this species as an input. The model estimated that 4 % of OC at the measurement site is associated with emissions of CG5.

The biogenic tracer serves to highlight that the posterior estimate does not differentiate between direct emissions at the source and chemical formation inside a plume associated with those direct emissions. The biogenic emissions are in the gas phase, and the model obtains an estimate of OC concentrations that results from them. The same applies for the individual source categories. For example the 19 % of impacts from the Other category are the sum of both direct emissions and chemical formation resulting from those emissions. A finer grained study using an aerosol module would be required to deconvolve these two processes.

For both the EC and OC inversion, we perform block-bootstrapping using 100 simulations with random selection of the days included in the analysis in order to estimate the uncertainties in the model results. For EC, the standard deviation of the contributions is between 5 % and 6 % of the mean contribution for all emission categories except for open burning where it is 20 %. For OC, the standard deviation is between 5 % and 15 % of the mean contribution for all emission categories. This suggests that the emissions estimates are robust with respect to uncertainties in the model inputs.

3.3 Inverse model results: temporal profiles

As described in Sect. 2.3, we performed the inversion using separate time series for 5 different time periods during the day, for weekdays and weekends, and for each month of the year. This led to $5 \times 2 \times 12$ entries in the inverse algorithm for each of 5 source types. We now present the monthly variation and the diurnal variation for emissions of EC and OC for each of the source types for weekdays and for weekends (which include Saturdays, Sundays and Holidays, SSH).

Figure 8 shows the monthly and diurnal temporal patterns for the On-Road emissions. 90 % confidence intervals on the inverse model results are shown on the graphs. These were obtained from the bootstrapping which provides an estimate of the uncertainty due to episode selection and transport errors, as discussed in Sect. 2.4. On-Road emissions are the category with the largest difference between inverse model results and the prior inventory.

In the prior for both EC and OC, weekday and weekend emissions are very similar, and there is only a slight annual variation from a maximum in the winter to a minimum in the summer months. The posterior levels for EC are similar to the emissions prior during the summer months for weekdays, but weekends are significantly lower. During Fall and Winter, the posterior emissions are very low, which explains why the total emission levels shown in Table 2 went from 4300 tpy in the prior to 2100 tpy in the posterior. The monthly variation of the OC posterior is similar to the EC posterior although total OC emissions are left relatively unchanged at around 2500 tpy. The large reduction in emissions during fall and winter is unlikely to be realistic, and so it suggests that there is an issue with the current representation of the emissions in the inventory and/or with the simulated wind transport from the sources to the receptor site.

The diurnal emissions profile of On-Road EC shows a sharp increase starting at 06:00 a.m., and a peak at 03:00–04:00 p.m. followed by a gradual decline until mid-night. There is a large contrast with the posterior. For weekdays EC follows the diurnal trend but has significantly lower emission levels, and has a strong reduction during

Title Page

Abstract

Introduction

Conclusions

References

Tables

Figures

◀

▶

◀

▶

Back

Close

Full Screen / Esc

Printer-friendly Version

Interactive Discussion



EC and OC inverse modeling

B. de Foy et al.

Title Page

Abstract

Introduction

Conclusions

References

Tables

Figures

◀

▶

◀

▶

Back

Close

Full Screen / Esc

Printer-friendly Version

Interactive Discussion



the afternoon rush hour. For weekends, there is very little diurnal variation of emissions. The OC posteriors follow the diurnal profile of the priors much more closely, with slightly higher emissions during the day and lower emissions on weekends than in the prior. It would therefore seem that OC On-Road emissions are better represented in the models than EC On-Road emissions.

Taken together, these results suggest that future research should seek to clarify the monthly profiles and the possibility of higher emissions during the summer rather than the winter. Furthermore, the posterior suggests that the diurnal profile could be improved as well as the difference between weekdays and weekends. It is possible that accuracy of the wind transport in the models is a function of the time of day, which could be a factor in the greater discrepancy between the prior and the posterior in the late afternoon. Finally, the large difference between the prior and the posterior could be the result of uncertainties in the current spatial distribution of the emissions.

In contrast to the On-Road emissions, the Non-Road posterior emissions follow the prior much more closely as can be seen in Fig. 9. There is a double peak, one in the early summer and a second one in the late fall. This confirms that simulations can be improved by taking into account the spring and fall maximum of agricultural equipment as was done in the LADCO inventory, rather than using the default summer maximum in MOVES.

For EC, the model suggests that there is a greater decrease in emissions on weekends than is currently represented in the inventory. The diurnal profile of the posterior follows that of the prior more closely than for the On-Road emissions, although there is again a sharp reduction of emissions in the posterior during the afternoon. The weekend emissions follow the diurnal profile, but are closer to 50 % lower than weekdays compared with 30 % lower in the priors.

For OC, the summer peak in the posterior is double that in the prior. This could be at least in part because the present study focuses on transport and does not include chemical formation. The summer peak could therefore be partly representative of OC formed in the plumes of Non-Road sources rather than a reflection of missing emis-

sions. This hypothesis is reinforced by the diurnal profile of the posterior which follows the prior except for an enhancement of nearly 50 % during the daylight hours.

The temporal profile of the MAR emissions (Marine/Aircraft/Railroad) are shown in Fig. 10. In the prior, these are the same for weekdays and weekends and vary by 30 % throughout the year from a minimum in winter to a maximum in the summer. The posterior for EC is similar in this respect, but has a more pronounced annual variations with lower emissions in the winter months. There are differences between weekdays and weekends, but these are not systematic and could be the result of model uncertainty. The same is true for OC, although the levels of OC are higher in the summer which could be due to chemical formation, as discussed for Non-Road emissions above.

The diurnal profile is flat in the prior, but the posterior suggests that there is a definite diurnal profile with emissions of EC at night lower than daytime levels by up to 50 %. There is less difference in the OC profile, but it still suggests that the diurnal activity profile should be reconsidered.

Other emissions are shown in Fig. 11. In the prior the winter time emissions are three times those during the summer for both EC and OC. This is in stark contrast to the posterior emissions. The inverse model finds that the EC concentrations at the receptor site are in good agreement with the emission patterns of spring through fall. No agreement is found however for the winter where the posterior estimate of both EC and OC emissions is nearly zero. For OC, the emissions are scaled up during the summer by a factor of 3 to 4, some of which is most likely due to chemical formation.

The diurnal profile of the Other category follows those of the On-Road emissions. For EC, the profile is similar although the emissions are much lower, and there is a reduction on weekends of morning emissions. For OC we see low posterior emissions at night and increased emissions during the day, as was the case for Non-Road emissions.

Finally, we see the temporal profiles for Point Sources in Fig. 12. The monthly emissions in the prior vary from a low in the spring to a high in the fall with about 30 % changes in EC but only 15 % in OC. This is roughly reproduced in the posterior for

EC and OC inverse modeling

B. de Foy et al.

Title Page

Abstract

Introduction

Conclusions

References

Tables

Figures

◀

▶

◀

▶

Back

Close

Full Screen / Esc

Printer-friendly Version

Interactive Discussion



EC and OC inverse modeling

B. de Foy et al.

Title Page

Abstract

Introduction

Conclusions

References

Tables

Figures

◀

▶

◀

▶

Back

Close

Full Screen / Esc

Printer-friendly Version

Interactive Discussion



EC albeit with a larger change from trough to peak. For OC, there are large swings in the emissions of the posterior. This suggests that there are large uncertainties in these estimates. From the perspective of the inverse model, it is a sign that there is poor agreement between the simulated and observed concentrations, but also that the estimates could be stabilized with more data.

The diurnal profile of the Point Sources is rather flat throughout the day in the prior. As for the MAR sources, the model suggests that there is a reduction in EC emissions between midnight and sunrise. There does also seem to be a slight reduction in EC emissions in the posterior on weekends compared with weekdays. The large swings in the estimates of monthly OC emissions mean that the diurnal profile should also be considered with caution. At a minimum, we can say that EC emissions from Point Sources seem to be reliably characterized in the inventory and the model, but that more research is needed for the OC impacts.

As discussed in Sect. 2.4, the WRF simulations do not have systematic errors for temperature, humidity, wind speed and direction at the surface. However, we do not have measurements of the mixing heights which could be used to evaluate errors in the vertical mixing in the model. In particular, these could contain systematic errors as a function of the time of day which would impact the diurnal profiles estimated by the inverse model. de Foy et al. (2007) found that the choice of the vertical mixing scheme in CAMx could have a significant impact on the estimation of emissions in Mexico City. This remains a source of uncertainty in the present analysis which could be constrained in future studies if more detailed measurements of the vertical structure of wind transport in the atmosphere became available.

3.4 Inverse model results: open burning

Section 3.2 showed that using emissions from FINN as the prior for CAMx simulations of open burning led to impacts of 1 % of EC and 3 % of OC. The posterior impacts were increased to 4 % for EC and 5 % for OC. Table 3 shows the emission totals by geographic sector in metric tonnes per year for the prior and for the posterior. For the

EC and OC inverse modeling

B. de Foy et al.

Title Page

Abstract

Introduction

Conclusions

References

Tables

Figures

◀

▶

◀

▶

Back

Close

Full Screen / Esc

Printer-friendly Version

Interactive Discussion



Local sector (within 100 km of the receptor), the northeast sector and the southeast sector, the inverse model increases the emissions by a factor of around 30 for EC and around 20 for OC. Emissions from the southwest sector are increased by a factor of 3 for EC and by a factor of 2 for OC. The open burning emissions from the west were kept at a similar level in the posterior as in the prior. The emissions from the northwest did not match the data and were set to 0 in the posterior by the inversion.

Table 3 also shows the posterior impact fractions by sector. The largest contributions are 1.4 % of EC and 2.5 % of OC from the southeast sector, followed by the southwest and the west sector. Local fires account for 0.7 % of EC and 0.5 % of OC in the posterior.

As discussed in Sect. 2.2, the emissions in FINN are based only on the Terra MODIS sensor, as the Aqua satellite was not yet in orbit in 2002. This means that the uncertainties in these emissions are greater than those following the launch of Aqua where there is twice as much satellite data available for fire detection (Hawbaker et al., 2008). In addition to missing fires, there are uncertainties in the estimates of area burned and of the type and amount of vegetation burned. Overall, these results suggest that the emission factors in FINN should be revised upwards.

3.5 Inverse model results: residence time analysis impacts

The inverse model combines emission estimates using Eulerian (CAMx) and Lagrangian (FLEXPART-WRF) simulations. Polar grids of Residence Time Analysis calculated using back-trajectories are used to estimate emission sources that could be missing in the LADCO emissions inventory. The polar gridded emissions have zero prior and represent a way of decomposing the residual between the CAMx posterior and the measurements into a spatial emission signal. The inverse model includes separate grids for 03:00 a.m. to 09:00 a.m., 09:00 a.m. to 03:00 p.m., 03:00 to 09:00 p.m. and 09:00 p.m. to 03:00 a.m., as well as for weekdays and weekends, for a total of 8 grids.

EC and OC inverse modeling

B. de Foy et al.

Title Page

Abstract

Introduction

Conclusions

References

Tables

Figures

◀

▶

◀

▶

Back

Close

Full Screen / Esc

Printer-friendly Version

Interactive Discussion



Figure 13 shows the sum of impacts from the 8 grids for both EC and OC. As shown in Fig. 7, these account for 33 % of the EC posterior time series and 46 % of the OC posterior time series. The main signal is from the south, and especially the southwest for both EC and OC, indicating that these could be areas to be explored for updating the spatial distribution of emissions.

Figure 14 shows the total contribution to the average concentration for EC and OC for each of the RTA grids. For EC, the contribution varies from a minimum of 0.05 ng m^{-3} to just above 0.25 ng m^{-3} . The contribution from the early morning to afternoon (03:00 a.m. to 03:00 p.m.) are lower than those for the late afternoon and nighttime (03:00 p.m. to 03:00 a.m.). The weekdays and weekends have a similar trends, but the diurnal variation is more pronounced on weekends. For OC, there is a similar pattern with lower contributions from 03:00 a.m. to 03:00 p.m., of around 0.8 ng m^{-3} rising to around 1.5 ng m^{-3} in the nighttime. Weekdays and weekends RTA impacts are more similar for OC than they are for EC.

3.6 Inverse model results: emission totals

In this section we compare the emissions in metric tonnes per year of the different source types from the inverse model with the NEI 2008 and the LADCO inventory. Table 2 and Fig. 15 show the annual total emissions for the St. Louis Regional domain for the 2008 National Emission Inventory, the 2007 LADCO inventory used as a prior, and for the posterior. Overall, the LADCO inventory is slightly larger than the NEI for both EC and OC. For EC, the On-Road emissions are 50 % larger, and the MAR emissions are 25 % larger while the remaining categories are similar. For OC, the largest category by far in both inventories are the Other sources. The LADCO inventory is slightly larger than the NEI, and combines residential wood and waste combustion, non-vehicle road emissions and food cooking (estimates of agricultural burning are high in the NEI but low in the LADCO inventory). OC emissions from On-Road, Non-Road, MAR and point sources are all increased by up to a factor of 2 in the LADCO inventory.

EC and OC inverse modeling

B. de Foy et al.

Title Page

Abstract

Introduction

Conclusions

References

Tables

Figures

◀

▶

◀

▶

Back

Close

Full Screen / Esc

Printer-friendly Version

Interactive Discussion



The posterior emissions are calculated from the model as departures from the LADCO prior. As discussed in Sect. 3.2, the simulated EC concentrations were too high at the site, and so the inverse model has lower emissions for all categories. The EC emission estimates from both On-Road sources and Other sources are reduced by 50% in the prior, whereas the remaining categories are only slightly reduced. For OC, there is only a slight reduction in the total emissions with a small shift in emissions from the Other category into Non-Road emissions. This suggests that the inverse results are in agreement with the inventory, bearing in mind that the model does not distinguish between primary and secondary OC. Comparison with Fig. 7 would suggest that the secondary OC is represented in the model by the polar grid emissions or as missing carbon rather than as adjustments to the known sources.

Also shown in Fig. 15 are annualized emissions for three time periods during the year that correspond to a natural grouping in the data: January to April, May to August and September to December. Compared with the LADCO inventory, the emissions estimates are low for January–April, high for May–August and similar for September–December. This shows that there is uncertainty in the model results that depends on the time of year and that in particular simulations are in greater disagreement with the inventories for January to April. At this stage it is not possible to say what part of this is due to limitations in the inventories, what part to measurements and especially what part due to modeling errors. Further research with more sites and longer time series would be able to better constrain the estimates.

4 Conclusions

A Least Squares Inverse model was used to estimate emissions of Elemental Carbon and Organic Carbon using hourly data for 2002 from the St. Louis-Midwest Super-site, and uncertainty estimates were obtained by running the model multiple times using block-bootstrapping. The model provided information on the diurnal pattern of the emissions, the difference between weekdays and weekends and the annual vari-

ation on a month by month basis. The inversion was based on the LADCO inventory for the following source types: On-Road, Non-Road, Marine/Aircraft/Railroad (MAR), Other and Point Sources.

The inverse emission estimates were in agreement with the LADCO inventory for most of the source types, with a slight downward revision of the emission totals. The main discrepancies suggested by the model are as follows: 1. On-Road emissions were poorly represented during the winter and on weekends. Although the results for winter remain as an outstanding question, there is a clear need to update the diurnal profile for weekends. 2. Non-Road emissions need to account for actual use of agricultural equipment, which was done by LADCO but is not carried out by default in MOVES. 3. MAR and Point sources do not at present have much diurnal variation in the emissions. Although their diurnal profiles are smoother than On-Road and Non-Road emissions, the model suggests that there is a discernible drop in nighttime emissions. 4. Other emissions from the inverse model matched the inventory during the summer but not during the winter. As with On-Road emissions, more research is required to constrain the sources of the discrepancy and to improve the simulations of these impacts.

In addition to these findings, the inverse model identified impacts from open burning at the measurement site, and suggests that emissions of EC and OC should be increased in the FINN model.

Finally, gridded back-trajectories suggest that most of the impacts missing from the emission inventories are due to transport from the quadrants southeast and southwest of the measurement site. The contributions to the average EC and OC concentrations at the measurement site from these sources are approximately twice as large during the late afternoon and early nighttime (03:00 p.m. to 03:00 a.m.) as they are earlier in the day (03:00 a.m. to 03:00 p.m.).

Acknowledgements. The United States Environmental Protection Agency (EPA) funded the EC and OC measurements used in this analysis through cooperative agreement R-82805901-0, and the analysis through grant number RD-83455701. Its contents are solely the responsibility of the grantee and do not necessarily represent the official views of the EPA. Further, the

EC and OC inverse modeling

B. de Foy et al.

Title Page

Abstract

Introduction

Conclusions

References

Tables

Figures

◀

▶

◀

▶

Back

Close

Full Screen / Esc

Printer-friendly Version

Interactive Discussion



EPA does not endorse the purchase of any commercial products or services mentioned in the publication. We thank the staff of the St. Louis-Midwest Fine-Particle Supersite for their assistance in data collection. We are also grateful to the US EPA for making the National Emissions Inventory Inventory available, and to the US National Climatic Data Center for the meteorological data.

References

- Akagi, S. K., Yokelson, R. J., Wiedinmyer, C., Alvarado, M. J., Reid, J. S., Karl, T., Crounse, J. D., and Wennberg, P. O.: Emission factors for open and domestic biomass burning for use in atmospheric models, *Atmos. Chem. Phys.*, 11, 4039–4072, doi:10.5194/acp-11-4039-2011, 2011. 12027
- Amato, F. and Hopke, P. K.: Source apportionment of the ambient PM_{2.5} across St. Louis using constrained positive matrix factorization, *Atmos. Environ.*, 46, 329–337, 2012. 12024
- Ashbaugh, L. L., Malm, W. C., and Sadeh, W. Z.: A residence time probability analysis of sulfur concentrations at grand-canyon-national-park, *Atmos. Environ.*, 19, 1263–1270, 1985. 12028
- Aster, R. C., Borchers, B., and Turber, C. H.: *Parameter Estimation and Inverse Problems*, 2nd edn., Academic Press, Oxford, UK, 2012. 12031
- Austin, E., Coull, B. A., Zanobetti, A., and Koutrakis, P.: A framework to spatially cluster air pollution monitoring sites in US based on the PM_{2.5} composition, *Environ. Int.*, 59, 244–254, 2013. 12024
- Bae, M. S., Schauer, J. J., DeMinter, J. T., and Turner, J. R.: Hourly and daily patterns of particle-phase organic and elemental carbon concentrations in the urban atmosphere, *J. Air Waste Manage.*, 54, 823–833, 2004a. 12023
- Bae, M. S., Schauer, J. J., DeMinter, J. T., Turner, J. R., Smith, D., and Cary, R. A.: Validation of a semi-continuous instrument for elemental carbon and organic carbon using a thermal-optical method, *Atmos. Environ.*, 38, 2885–2893, 2004b. 12023, 12025
- Bae, M. S., Schauer, J. J., and Turner, J. R.: Estimation of the monthly average ratios of organic mass to organic carbon for fine particulate matter at an urban site, *Aerosol Sci. Tech.*, 40, 1123–1139, 2006. 12023

EC and OC inverse modeling

B. de Foy et al.

Title Page

Abstract

Introduction

Conclusions

References

Tables

Figures

◀

▶

◀

▶

Back

Close

Full Screen / Esc

Printer-friendly Version

Interactive Discussion



EC and OC inverse modeling

B. de Foy et al.

Title Page

Abstract

Introduction

Conclusions

References

Tables

Figures

◀

▶

◀

▶

Back

Close

Full Screen / Esc

Printer-friendly Version

Interactive Discussion



Bell, M. L., Ebisu, K., Peng, R. D., Samet, J. M., and Dominici, F.: Hospital admissions and chemical composition of fine particle air pollution, *Am. J. Resp. Crit. Care*, 179, 1115–1120, 2009. 12022

Bond, T. C., Doherty, S. J., Fahey, D. W., Forster, P. M., Berntsen, T., DeAngelo, B. J., Flanner, M. G., Ghan, S., Kaercher, B., Koch, D., Kinne, S., Kondo, Y., Quinn, P. K., Sarofim, M. C., Schultz, M. G., Schulz, M., Venkataraman, C., Zhang, H., Zhang, S., Bellouin, N., Gutikunda, S. K., Hopke, P. K., Jacobson, M. Z., Kaiser, J. W., Klimont, Z., Lohmann, U., Schwarz, J. P., Shindell, D., Storelvmo, T., Warren, S. G., and Zender, C. S.: Bounding the role of black carbon in the climate system: a scientific assessment, *J. Geophys. Res.-Atmos.*, 118, 5380–5552, 2013. 12022

Brioude, J., Kim, S.-W., Angevine, W. M., Frost, G. J., Lee, S.-H., McKeen, S. A., Trainer, M., Fehsenfeld, F. C., Holloway, J. S., Ryerson, T. B., Williams, E. J., Petron, G., and Fast, J. D.: Top-down estimate of anthropogenic emission inventories and their interannual variability in Houston using a mesoscale inverse modeling technique, *J. Geophys. Res.-Atmos.*, 116, D20305, doi:10.1029/2011JD016215, 2011. 12029

Brioude, J., Angevine, W. M., Ahmadov, R., Kim, S.-W., Evan, S., McKeen, S. A., Hsie, E.-Y., Frost, G. J., Neuman, J. A., Pollack, I. B., Peischl, J., Ryerson, T. B., Holloway, J., Brown, S. S., Nowak, J. B., Roberts, J. M., Wofsy, S. C., Santoni, G. W., Oda, T., and Trainer, M.: Top-down estimate of surface flux in the Los Angeles Basin using a mesoscale inverse modeling technique: assessing anthropogenic emissions of CO, NO_x and CO₂ and their impacts, *Atmos. Chem. Phys.*, 13, 3661–3677, doi:10.5194/acp-13-3661-2013, 2013. 12029

Brioude, J., Arnold, D., Stohl, A., Cassiani, M., Morton, D., Seibert, P., Angevine, W., Evan, S., Dingwell, A., Fast, J. D., Easter, R. C., Pisso, I., Burkhardt, J., and Wotawa, G.: The Lagrangian particle dispersion model FLEXPART-WRF version 3.1, *Geosci. Model Dev.*, 6, 1889–1904, doi:10.5194/gmd-6-1889-2013, 2013b. 12028

Brunner, D., Henne, S., Keller, C. A., Reimann, S., Vollmer, M. K., O'Doherty, S., and Maione, M.: An extended Kalman-filter for regional scale inverse emission estimation, *Atmos. Chem. Phys.*, 12, 3455–3478, doi:10.5194/acp-12-3455-2012, 2012. 12030

Carroll, M., Townshend, J., Hansen, M., DiMiceli, C., Sohlberg, R., and Wurster, K.: Vegetative cover conversion and vegetation continuous fields, in: *Land Remote Sensing and Global Environmental Change: NASA's Earth Observing System and the Science of Aster and MODIS*, edited by: Ramachandran, B., Justice, C. O., and Abrams, M., Springer-Verlag, New York, NY, 725–746, 2011. 12027

EC and OC inverse modeling

B. de Foy et al.

[Title Page](#)[Abstract](#)[Introduction](#)[Conclusions](#)[References](#)[Tables](#)[Figures](#)[◀](#)[▶](#)[◀](#)[▶](#)[Back](#)[Close](#)[Full Screen / Esc](#)[Printer-friendly Version](#)[Interactive Discussion](#)

- de Foy, B., Lei, W., Zavala, M., Volkamer, R., Samuelsson, J., Mellqvist, J., Galle, B., Martínez, A.-P., Grutter, M., Retama, A., and Molina, L. T.: Modelling constraints on the emission inventory and on vertical dispersion for CO and SO₂ in the Mexico City Metropolitan Area using Solar FTIR and zenith sky UV spectroscopy, *Atmos. Chem. Phys.*, 7, 781–801, doi:10.5194/acp-7-781-2007, 2007. 12029, 12041
- de Foy, B., Zavala, M., Bei, N., and Molina, L. T.: Evaluation of WRF mesoscale simulations and particle trajectory analysis for the MILAGRO field campaign, *Atmos. Chem. Phys.*, 9, 4419–4438, doi:10.5194/acp-9-4419-2009, 2009. 12029
- de Foy, B., Smyth, A. M., Thompson, S. L., Gross, D. S., Olson, M. R., Sager, N., and Schauer, J. J.: Sources of nickel, vanadium and black carbon in aerosols in Milwaukee, *Atmos. Environ.*, 59, 294–301, 2012a. 12023
- de Foy, B., Wiedinmyer, C., and Schauer, J. J.: Estimation of mercury emissions from forest fires, lakes, regional and local sources using measurements in Milwaukee and an inverse method, *Atmos. Chem. Phys.*, 12, 8993–9011, doi:10.5194/acp-12-8993-2012, 2012b. 12028, 12029, 12031
- de Foy, B., Heo, J., and Schauer, J. J.: Estimation of direct emissions and atmospheric processing of reactive mercury using inverse modeling, *Atmos. Environ.*, 85, 73–82, 2014. 12028, 12029, 12033
- Efron, B.: Bayes' theorem in the 21st century, *Science*, 340, 1177–1178, 2013. 12032
- ENVIRON: CAMx User's Guide, Comprehensive Air quality Model with eXtensions, Tech. Rep. Version 6.0, ENVIRON International Corporation, Novato, CA, 2013. 12029
- EPA, U.: Motor Vehicle Emissions Simulator (MOVES), Tech. Rep. EPA-420-B-12-001b, US EPA, Research Triangle Park, NC, 2012. 12026
- Friedl, M. A., Sulla-Menashe, D., Tan, B., Schneider, A., Ramankutty, N., Sibley, A., and Huang, X.: MODIS Collection 5 global land cover: algorithm refinements and characterization of new datasets, *Remote Sens. Environ.*, 114, 168–182, 2010. 12027
- Gentner, D. R., Isaacman, G., Worton, D. R., Chan, A. W., Dallmann, T. R., Davis, L., Liu, S., Day, D. A., Russell, L. M., Wilson, K. R., Weber, R., Guha, A., Harley, R. A., and Goldstein, A. H.: Elucidating secondary organic aerosol from diesel and gasoline vehicles through detailed characterization of organic carbon emissions, *P. Natl. Acad. Sci.*, 109, 18318–18323, 2012. 12023
- Giglio, L., Descloitres, J., Justice, C., and Kaufman, Y.: An enhanced contextual fire detection algorithm for MODIS, *Remote Sens. Environ.*, 87, 273–282, 2003. 12027

EC and OC inverse modeling

B. de Foy et al.

Title Page

Abstract

Introduction

Conclusions

References

Tables

Figures

◀

▶

◀

▶

Back

Close

Full Screen / Esc

Printer-friendly Version

Interactive Discussion



- Guenther, A., Karl, T., Harley, P., Wiedinmyer, C., Palmer, P. I., and Geron, C.: Estimates of global terrestrial isoprene emissions using MEGAN (Model of Emissions of Gases and Aerosols from Nature), *Atmos. Chem. Phys.*, 6, 3181–3210, doi:10.5194/acp-6-3181-2006, 2006. 12026
- 5 Hand, J. L., Schichtel, B. A., Pitchford, M., Malm, W. C., and Frank, N. H.: Seasonal composition of remote and urban fine particulate matter in the United States, *J. Geophys. Res.-Atmos.*, 117, D05209, doi:10.1029/2011JD017122, 2012. 12022
- Hand, J. L., Schichtel, B. A., Malm, W. C., and Frank, N. H.: Spatial and temporal trends in PM_{2.5} organic and elemental carbon across the United States, *Advances in Meteorology*, 2013, 367674, doi:10.1155/2013/367674, 2013. 12022
- 10 Hansen, M. C., Townshend, J. R. G., Defries, R. S., and Carroll, M.: Estimation of tree cover using MODIS data at global, continental and regional/local scales, *Int. J. Remote Sens.*, 26, 4359–4380, 2005. 12027
- Hansen, M. C., DeFries, R. S., Townshend, J. R. G., Carroll, M., Dimiceli, C., and Sohlberg, R. A.: Global percent tree cover at a spatial resolution of 500 meters: first results of the MODIS vegetation continuous fields algorithm, *Earth Interact.*, 7, 1–15, 2003. 12027
- 15 Hawbaker, T. J., Radeloff, V. C., Syphard, A. D., Zhu, Z., and Stewart, S. I.: Detection rates of the MODIS active fire product in the United States, *Remote Sens. Environ.*, 112, 2656–2664, 2008. 12027, 12042
- Henze, D. K., Seinfeld, J. H., and Shindell, D. T.: Inverse modeling and mapping US air quality influences of inorganic PM_{2.5} precursor emissions using the adjoint of GEOS-Chem, *Atmos. Chem. Phys.*, 9, 5877–5903, doi:10.5194/acp-9-5877-2009, 2009. 12032
- Hoelzemann, J., Schultz, M., Brasseur, G., Granier, C., and Simon, M.: Global Wildland Fire Emission Model (GWEM): evaluating the use of global area burnt satellite data, *J. Geophys. Res.-Atmos.*, 109, D14S04, doi:10.1029/2003JD003666, 2004. 12027
- 25 Jaeckels, J. M., Bae, M.-S., and Schauer, J. J.: Positive matrix factorization (PMF) analysis of molecular marker measurements to quantify the sources of organic aerosols, *Environ. Sci. Technol.*, 41, 5763–5769, 2007. 12023
- 30 Jimenez, J. L., Canagaratna, M. R., Donahue, N. M., Prevot, A. S. H., Zhang, Q., Kroll, J. H., DeCarlo, P. F., Allan, J. D., Coe, H., Ng, N. L., Aiken, A. C., Docherty, K. S., Ulbrich, I. M., Grieshop, A. P., Robinson, A. L., Duplissy, J., Smith, J. D., Wilson, K. R., Lanz, V. A., Hueglin, C., Sun, Y. L., Tian, J., Laaksonen, A., Raatikainen, T., Rautiainen, J., Vaatto-

EC and OC inverse modeling

B. de Foy et al.

Title Page

Abstract

Introduction

Conclusions

References

Tables

Figures

◀

▶

◀

▶

Back

Close

Full Screen / Esc

Printer-friendly Version

Interactive Discussion



vaara, P., Ehn, M., Kulmala, M., Tomlinson, J. M., Collins, D. R., Cubison, M. J., Dunlea, E. J., Huffman, J. A., Onasch, T. B., Alfarra, M. R., Williams, P. I., Bower, K., Kondo, Y., Schneider, J., Drewnick, F., Borrmann, S., Weimer, S., Demerjian, K., Salcedo, D., Cottrell, L., Griffin, R., Takami, A., Miyoshi, T., Hatakeyama, S., Shimono, A., Sun, J. Y., Zhang, Y. M., Dzepina, K., Kimmel, J. R., Sueper, D., Jayne, J. T., Herndon, S. C., Trimborn, A. M., Williams, L. R., Wood, E. C., Middlebrook, A. M., Kolb, C. E., Baltensperger, U., and Worsnop, D. R.: Evolution of organic aerosols in the atmosphere, *Science*, 326, 1525–1529, 2009. 12022

LADCO: Regional Air Quality Analyses for Ozone, PM_{2.5}, and Regional Haze: Base C Emissions Inventory, Tech. Rep. 12 September 2011, Lake Michigan Air Directors Consortium, Rosemont, IL, 2011. 12025, 12026

Lee, J. H. and Hopke, P. K.: Apportioning sources of PM_{2.5} in St. Louis, MO using speciation trends network data, *Atmos. Environ.*, 40, S360–S377, 2006. 12024

Lee, J. H., Hopke, P. K., and Turner, J. R.: Source identification of airborne PM_{2.5} at the St. Louis-Midwest Supersite, *J. Geophys. Res.-Atmos.*, 111, D10S10, doi:10.1029/2002JD006329, 2006. 12024

Lewandowski, M., Jaoui, M., Offenberg, J. H., Kleindienst, T. E., Edney, E. O., Sheesley, R. J., and Schauer, J. J.: Primary and secondary contributions to ambient PM in the midwestern United States, *Environ. Sci. Technol.*, 42, 3303–3309, 2008. 12022

Lin, J., Gerbig, C., Wofsy, S., Andrews, A., Daube, B., Davis, K., and Grainger, C.: A near-field tool for simulating the upstream influence of atmospheric observations: the Stochastic Time-Inverted Lagrangian Transport (STILT) model, *J. Geophys. Res.-Atmos.*, 108, 4493, doi:10.1029/2002JD003161, 2003. 12028

Mesinger, F., DiMego, G., Kalnay, E., Mitchell, K., Shafran, P., Ebisuzaki, W., Jovic, D., Woollen, J., Rogers, E., Berbery, E., Ek, M., Fan, Y., Grumbine, R., Higgins, W., Li, H., Lin, Y., Manikin, G., Parrish, D., and Shi, W.: North American regional reanalysis, *B. Am. Meteorol. Soc.*, 87, 343–360, doi:10.1175/BAMS-87-3-343, 2006. 12028

Miller, S. M., Michalak, A. M., and Levi, P. J.: Atmospheric inverse modeling with known physical bounds: an example from trace gas emissions, *Geosci. Model Dev.*, 7, 303–315, doi:10.5194/gmd-7-303-2014, 2014. 12033

Napelenok, S. L., Simon, H., Bhawe, P. V., Pye, H. O. T., Pouliot, G. A., Sheesley, R. J., and Schauer, J. J.: Diagnostic air quality model evaluation of source-specific primary and secondary fine particulate carbon, *Environ. Sci. Technol.*, 48, 464–473, 2014. 12022, 12023

EC and OC inverse modeling

B. de Foy et al.

Title Page

Abstract

Introduction

Conclusions

References

Tables

Figures

◀

▶

◀

▶

Back

Close

Full Screen / Esc

Printer-friendly Version

Interactive Discussion



- Ramanathan, V. and Carmichael, G.: Global and regional climate changes due to black carbon, *Nat. Geosci.*, 1, 221–227, 2008. 12022
- Reche, C., Querol, X., Alastuey, A., Viana, M., Pey, J., Moreno, T., Rodríguez, S., González, Y., Fernández-Camacho, R., de la Rosa, J., Dall'Osto, M., Prévôt, A. S. H., Hueglin, C., Harrison, R. M., and Quincey, P.: New considerations for PM, Black Carbon and particle number concentration for air quality monitoring across different European cities, *Atmos. Chem. Phys.*, 11, 6207–6227, doi:10.5194/acp-11-6207-2011, 2011. 12023
- Rigby, M., Manning, A. J., and Prinn, R. G.: Inversion of long-lived trace gas emissions using combined Eulerian and Lagrangian chemical transport models, *Atmos. Chem. Phys.*, 11, 9887–9898, doi:10.5194/acp-11-9887-2011, 2011. 12029
- Robinson, A. L., Donahue, N. M., Shrivastava, M. K., Weitkamp, E. A., Sage, A. M., Grieshop, A. P., Lane, T. E., Pierce, J. R., and Pandis, S. N.: Rethinking organic aerosols: semivolatile emissions and photochemical aging, *Science*, 315, 1259–1262, 2007. 12022
- Rödenbeck, C., Gerbig, C., Trusilova, K., and Heimann, M.: A two-step scheme for high-resolution regional atmospheric trace gas inversions based on independent models, *Atmos. Chem. Phys.*, 9, 5331–5342, doi:10.5194/acp-9-5331-2009, 2009. 12029
- Rohr, A. C. and Wyzga, R. E.: Attributing health effects to individual particulate matter constituents, *Atmos. Environ.*, 62, 130–152, 2012. 12022
- Seibert, P. and Frank, A.: Source-receptor matrix calculation with a Lagrangian particle dispersion model in backward mode, *Atmos. Chem. Phys.*, 4, 51–63, doi:10.5194/acp-4-51-2004, 2004. 12028
- Seibert, P., Kromp-Kolb, H., Baltensperger, U., Jost, D. T., and Schwikowski, M.: Trajectory analysis of high-alpine air pollution data, in: *Air Pollution Modelling and its Application X*, edited by: Gryning, S.-E. and Millan, M. M., Plenum Press, New York, 595–596, 1994. 12029
- Sheesley, R. J., Schauer, J. J., Meiritz, M., DeMinter, J. T., Bae, M.-S., and Turner, J. R.: Daily variation in particle-phase source tracers in an urban atmosphere, *Aerosol Sci. Tech.*, 41, 981–993, 2007. 12023
- Skamarock, W. C., Klemp, J. B., Dudhia, J., Gill, D. O., Barker, D. M., Wang, W., and Powers, J. G.: A Description of the Advanced Research WRF Version 2, Tech. Rep. NCAR/TN-468+STR, NCAR, Boulder, CO, 2005. 12028
- Snyder, D. C., Schauer, J. J., Gross, D. S., and Turner, J. R.: Estimating the contribution of point sources to atmospheric metals using single-particle mass spectrometry, *Atmos. Environ.*, 43, 4033–4042, 2009. 12035

EC and OC inverse modeling

B. de Foy et al.

[Title Page](#)[Abstract](#)[Introduction](#)[Conclusions](#)[References](#)[Tables](#)[Figures](#)[◀](#)[▶](#)[◀](#)[▶](#)[Back](#)[Close](#)[Full Screen / Esc](#)[Printer-friendly Version](#)[Interactive Discussion](#)

- Snyder, D. C., Rutter, A. P., Worley, C., Olson, M., Plourde, A., Bader, R. C., Dallmann, T., and Schauer, J. J.: Spatial variability of carbonaceous aerosols and associated source tracers in two cities in the Midwestern United States, *Atmos. Environ.*, 44, 1597–1608, 2010. 12022
- Spak, S. N., and Holloway, T.: Seasonality of speciated aerosol transport over the Great Lakes region, *J. Geophys. Res.-Atmos.*, 114, D08302, doi:10.1029/2008JD010598, 2009. 12022
- Stohl, A., Forster, C., Frank, A., Seibert, P., and Wotawa, G.: Technical note: The Lagrangian particle dispersion model FLEXPART version 6.2, *Atmos. Chem. Phys.*, 5, 2461–2474, doi:10.5194/acp-5-2461-2005, 2005. 12028
- Stohl, A., Seibert, P., Arduini, J., Eckhardt, S., Fraser, P., Grealley, B. R., Lunder, C., Maione, M., Mühle, J., O'Doherty, S., Prinn, R. G., Reimann, S., Saito, T., Schmidbauer, N., Simmonds, P. G., Vollmer, M. K., Weiss, R. F., and Yokouchi, Y.: An analytical inversion method for determining regional and global emissions of greenhouse gases: Sensitivity studies and application to halocarbons, *Atmos. Chem. Phys.*, 9, 1597–1620, doi:10.5194/acp-9-1597-2009, 2009. 12029, 12031
- Sullivan, A. P., Weber, R. J., Clements, A. L., Turner, J. R., Bae, M. S., and Schauer, J. J.: A method for on-line measurement of water-soluble organic carbon in ambient aerosol particles: results from an urban site, *Geophys. Res. Lett.*, 31, L13105, doi:10.1029/2004GL019681, 2004. 12023
- Wang, G., Hopke, P. K., and Turner, J. R.: Using highly time resolved fine particulate compositions to find particle sources in St. Louis, MO, *Atmospheric Pollution Research*, 2, 219–230, 2011. 12024
- Wiedinmyer, C., Akagi, S. K., Yokelson, R. J., Emmons, L. K., Al-Saadi, J. A., Orlando, J. J., and Soja, A. J.: The Fire INventory from NCAR (FINN): a high resolution global model to estimate the emissions from open burning, *Geosci. Model Dev.*, 4, 625–641, doi:10.5194/gmd-4-625-2011, 2011. 12027
- Wunsch, C.: *Discrete Inverse and State Estimation Problems: With Geophysical Fluid Applications*, Cambridge University Press, Cambridge, UK, 2006. 12031

EC and OC inverse modeling

B. de Foy et al.

Title Page

Abstract

Introduction

Conclusions

References

Tables

Figures

◀

▶

◀

▶

Back

Close

Full Screen / Esc

Printer-friendly Version

Interactive Discussion



Table 1. Pearson’s correlation coefficient squared for simulated time series of EC and OC for the complete time series as well as for the subset of points included in the inversion after the Iteratively Reweighted Least Squares (IRLS) procedure. The full inverse time series is the sum of the CAMx posterior and the impacts due to the gridded back-trajectories.

r^2	Elemental Carbon		Organic Carbon	
	All Points	IRLS Points	All Points	IRLS Points
CAMx Prior	0.11	0.19	0.07	0.10
CAMx Posterior	0.28	0.37	0.26	0.29
Full Inverse	0.42	0.53	0.47	0.56

EC and OC inverse modeling

B. de Foy et al.

Table 3. Emission totals for open burning by geographical sector relative to the measurement site for the FINN model and the Least Squares Inverse model. Also shown are the ratios of the Inverse emission estimates to the FINN prior estimates and the fraction of EC or OC at the measurement site that is estimated to be due to open burning.

Sector	Elemental Carbon				Organic Carbon			
	FINN tpy	Inverse tpy	Ratio	Impact %	FINN tpy	Inverse tpy	Ratio	Impact %
Local – 100 km	173	4708	27.27	0.69	1508	21 696	14.39	0.47
Northeast	553	14 031	25.37	0.18	6430	130 196	20.25	0.22
Southeast	5088	180 228	35.42	1.36	66 187	1 541 067	23.28	2.53
Southwest	3714	11 749	3.16	0.86	48 028	103 156	2.15	1.63
West	558	592	1.06	0.82	4149	3611	0.87	1.00
Northwest	459	0	0.00	0.00	2899	0	0.00	0.00
Total	10 577	211 309	20.0	3.5	129 409	1 799 725	13.9	5.1

[Title Page](#)
[Abstract](#)
[Introduction](#)
[Conclusions](#)
[References](#)
[Tables](#)
[Figures](#)
[◀](#)
[▶](#)
[◀](#)
[▶](#)
[Back](#)
[Close](#)
[Full Screen / Esc](#)
[Printer-friendly Version](#)
[Interactive Discussion](#)


EC and OC inverse modeling

B. de Foy et al.

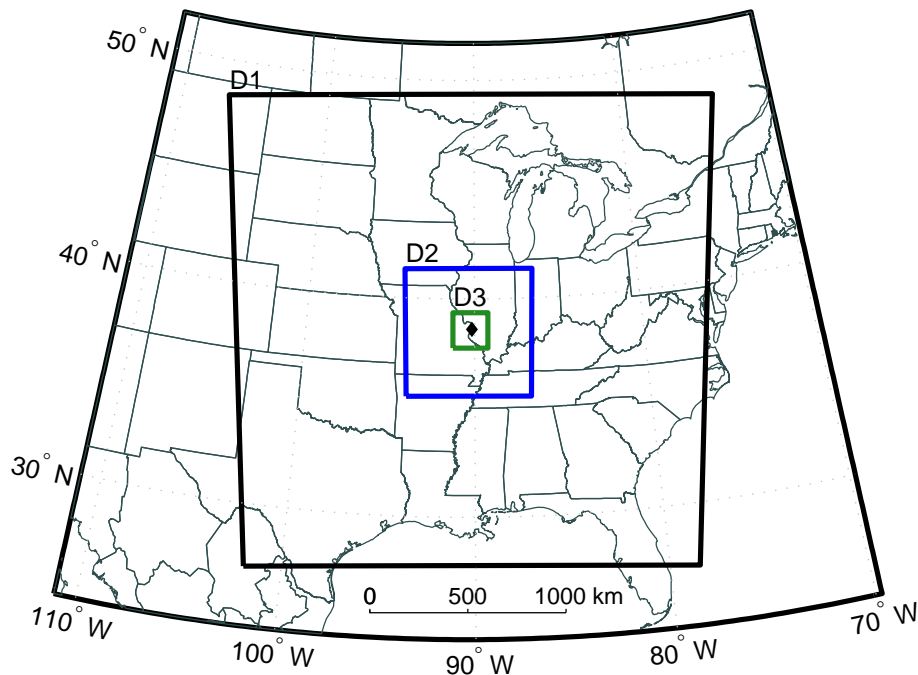


Fig. 1. Domains used for the WRF simulations: large (D1, 27 km resolution), Regional (D2, 9 km resolution) and Local (D3, 3 km resolution). CAMx simulations are performed on the Regional and Local domains, except for open burning which are performed on the Large and the Regional domains. The diamond shows the location of the St. Louis-Midwest Supersite.

[Title Page](#)[Abstract](#)[Introduction](#)[Conclusions](#)[References](#)[Tables](#)[Figures](#)[◀](#)[▶](#)[◀](#)[▶](#)[Back](#)[Close](#)[Full Screen / Esc](#)[Printer-friendly Version](#)[Interactive Discussion](#)

EC and OC inverse modeling

B. de Foy et al.

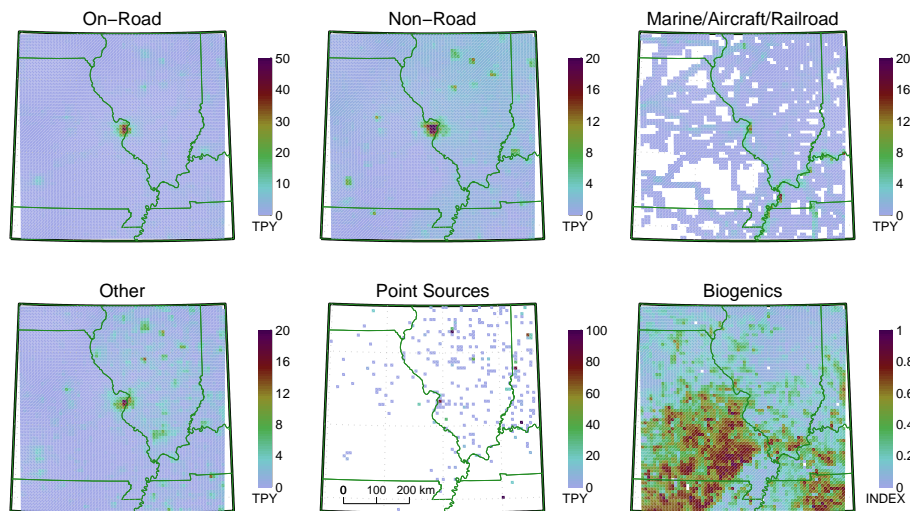


Fig. 2. Elemental Carbon emissions by source type from the LADCO inventory for the Regional domain in metric tonnes per year, and biogenic tracer emissions in non-dimensional units.

Title Page

Abstract Introduction

Conclusions References

Tables Figures

◀ ▶

◀ ▶

Back Close

Full Screen / Esc

Printer-friendly Version

Interactive Discussion



EC and OC inverse modeling

B. de Foy et al.

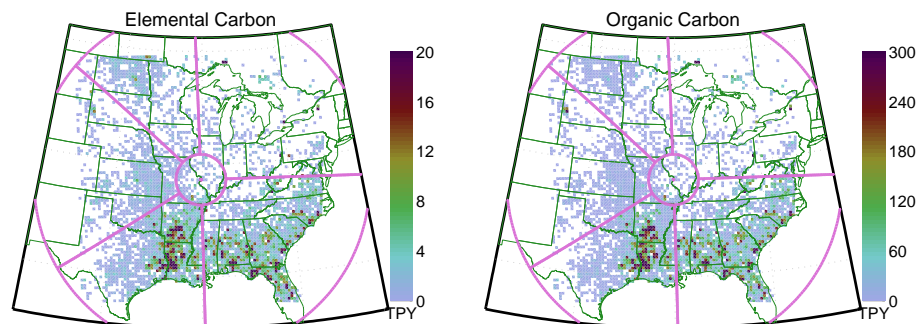


Fig. 3. Open burning emissions of EC and OC for the Large domain for 2002 using the FINN model, which include forest, prescribed and agricultural fires detected by Terra MODIS. Pink lines show the 6 sectors used in the inverse model, pink dot is the supersite.

[Title Page](#)[Abstract](#)[Introduction](#)[Conclusions](#)[References](#)[Tables](#)[Figures](#)[◀](#)[▶](#)[◀](#)[▶](#)[Back](#)[Close](#)[Full Screen / Esc](#)[Printer-friendly Version](#)[Interactive Discussion](#)

EC and OC inverse modeling

B. de Foy et al.

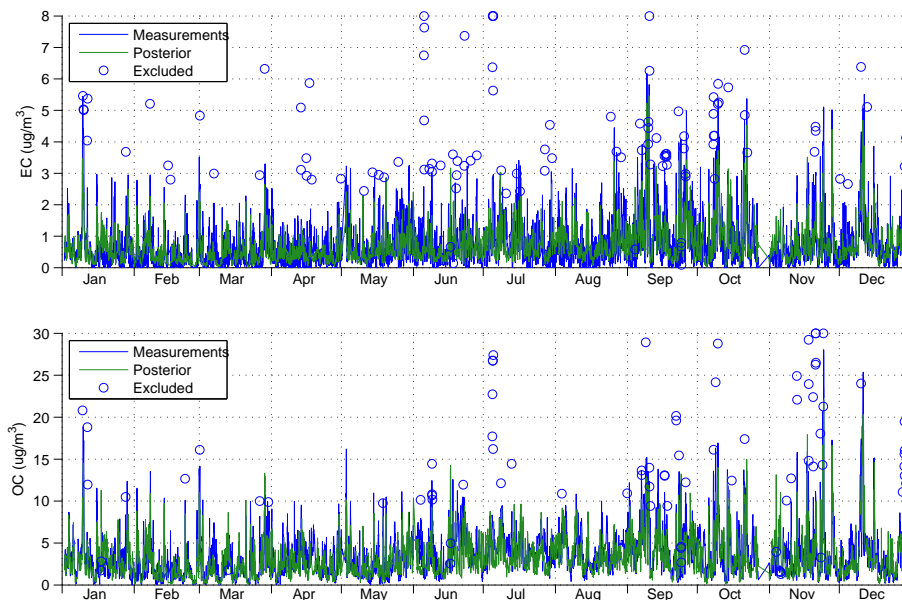


Fig. 4. Time series of Elemental and Organic Carbon at the St. Louis-Midwest supersite for 2002. Measurements are shown in blue, circles show the data points excluded from the analysis by the Iteratively Reweighted Least Squares scheme. Green line shows the posterior time series, as produced by the Least Squares Inverse model.

[Title Page](#)[Abstract](#)[Introduction](#)[Conclusions](#)[References](#)[Tables](#)[Figures](#)[◀](#)[▶](#)[◀](#)[▶](#)[Back](#)[Close](#)[Full Screen / Esc](#)[Printer-friendly Version](#)[Interactive Discussion](#)

EC and OC inverse modeling

B. de Foy et al.

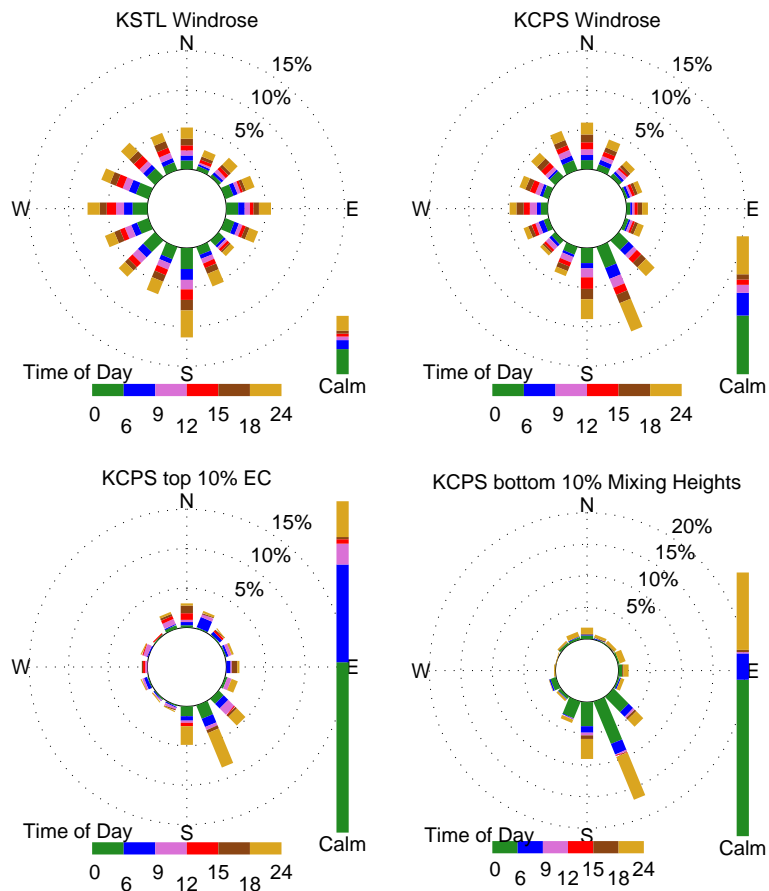


Fig. 5. Top: wind roses for Lambert – St. Louis international airport (KSTL) and Downtown St. Louis airport (KCPS). Bottom: wind roses for hours in the top 10 % of EC concentrations at the supersite using KCPS data, and bottom 10 % of WRF mixing layer height. Color indicates time of day.

EC and OC inverse modeling

B. de Foy et al.

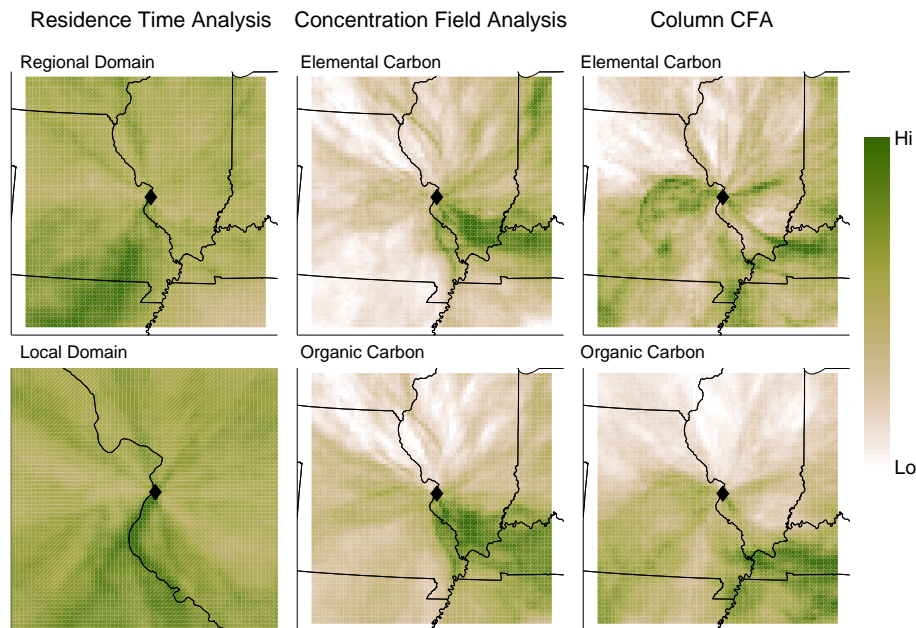


Fig. 6. Left: Residence Time Analysis of FLEXPART-WRF back-trajectories using hourly releases during 2002 showing the origin of air masses arriving at the supersite (diamond). Center: Concentration Field Analysis of EC and OC showing air mass transport associated with peak concentrations. Right: Column Concentration Field Analysis of EC and OC showing air mass transport associated with higher column amounts of EC and OC.

[Full Screen / Esc](#)[Printer-friendly Version](#)[Interactive Discussion](#)

EC and OC inverse modeling

B. de Foy et al.

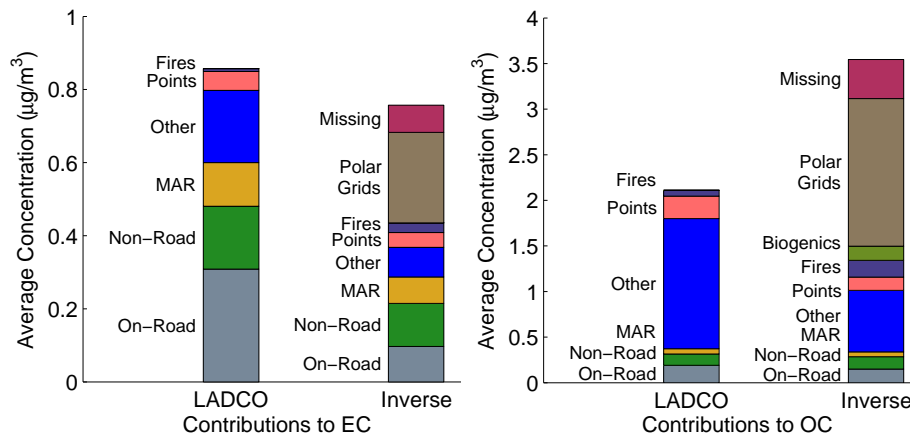


Fig. 7. Contributions of different types of sources to the average concentration of EC and OC at the St. Louis-Midwest Supersite using the LADCO inventory (prior) and the Least Squares Inverse model (posterior).

Title Page

Abstract

Introduction

Conclusions

References

Tables

Figures

◀

▶

◀

▶

Back

Close

Full Screen / Esc

Printer-friendly Version

Interactive Discussion



EC and OC inverse modeling

B. de Foy et al.

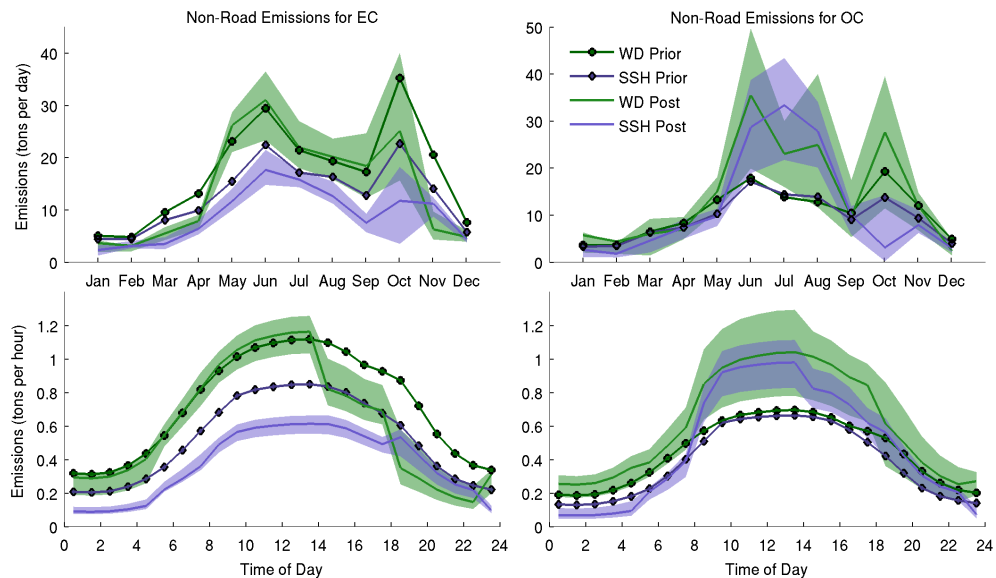


Fig. 9. Monthly and diurnal temporal pattern of emissions of EC and OC for Non-Road emissions by weekday and weekend for the St. Louis region, see Fig. 8.

Title Page

Abstract Introduction

Conclusions References

Tables Figures

◀ ▶

◀ ▶

Back Close

Full Screen / Esc

Printer-friendly Version

Interactive Discussion



EC and OC inverse modeling

B. de Foy et al.

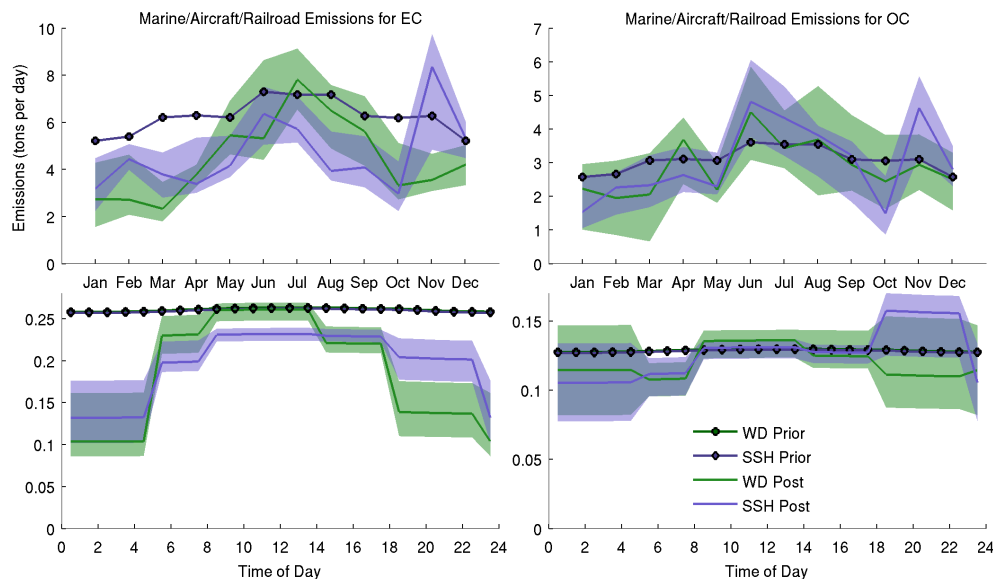


Fig. 10. Monthly and diurnal temporal pattern of emissions of EC and OC for Marine/Aircraft/Railroad (MAR) emissions by weekday and weekend for the St. Louis region, see Fig. 8.

Title Page

Abstract Introduction

Conclusions References

Tables Figures

◀ ▶

◀ ▶

Back Close

Full Screen / Esc

Printer-friendly Version

Interactive Discussion



EC and OC inverse modeling

B. de Foy et al.

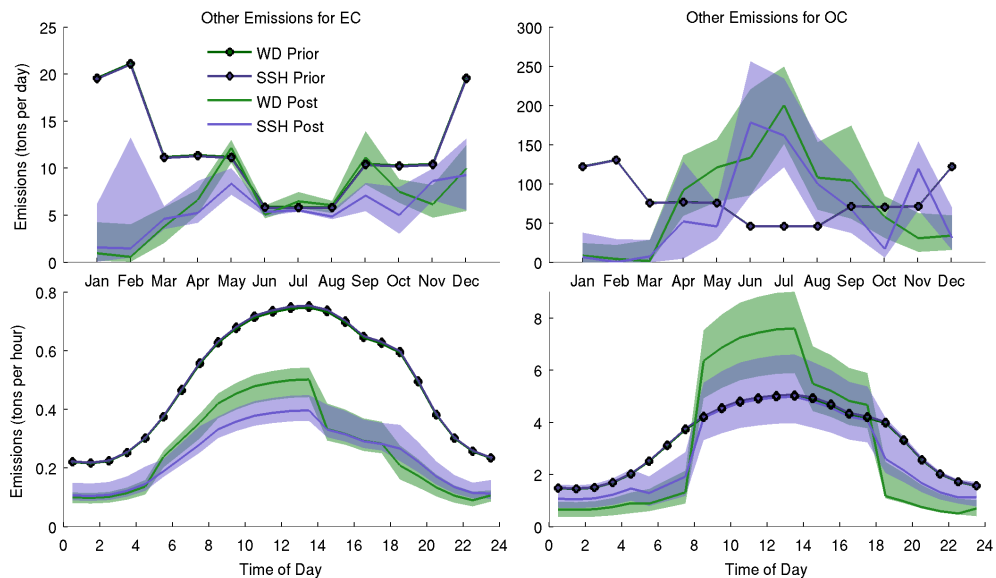


Fig. 11. Monthly and diurnal temporal pattern of emissions of EC and OC for “Other” emissions by weekday and weekend for the St. Louis region, see Fig. 8.

Title Page

Abstract Introduction

Conclusions References

Tables Figures

◀ ▶

◀ ▶

Back Close

Full Screen / Esc

Printer-friendly Version

Interactive Discussion



EC and OC inverse modeling

B. de Foy et al.

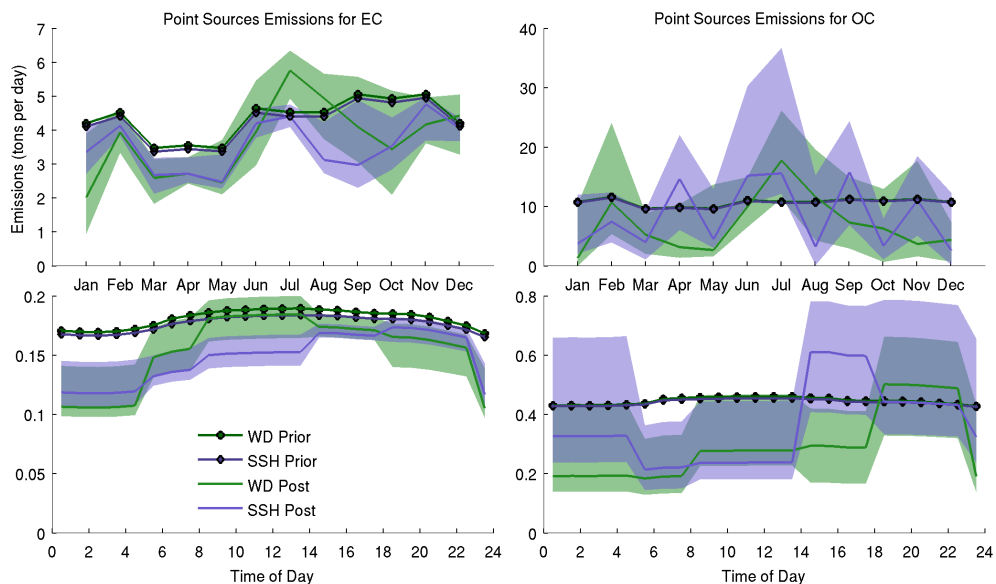


Fig. 12. Monthly and diurnal temporal pattern of emissions of EC and OC for Point Source emissions by weekday and weekend for the St. Louis region, see Fig. 8.

Title Page

Abstract Introduction

Conclusions References

Tables Figures

◀ ▶

◀ ▶

Back Close

Full Screen / Esc

Printer-friendly Version

Interactive Discussion



EC and OC inverse modeling

B. de Foy et al.

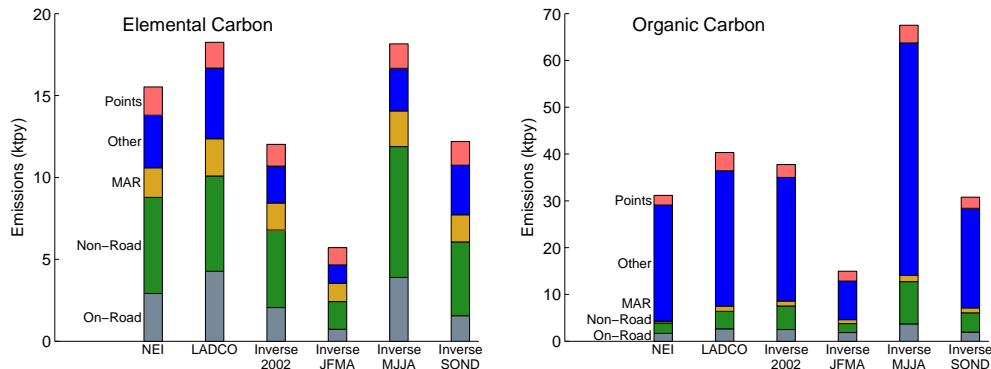


Fig. 15. Emissions of EC and OC in the Regional domain by source type for the 2008 NEI, the 2007 LADCO inventory and the posterior estimate based on using LADCO as a prior. Inverse results are shown for the entire year (2002), along with annualized emissions for January–April (JFMA), May–August (MJJA) and September–December (SOND).

Title Page

Abstract

Introduction

Conclusions

References

Tables

Figures

⏪

⏩

◀

▶

Back

Close

Full Screen / Esc

Printer-friendly Version

Interactive Discussion

